

## Magnetic property applications of microwave method prepared zinc ion modified $\text{CoAl}_2\text{O}_4$ nanoparticles

C. S. Dash<sup>a</sup>, M. Kamalakannan<sup>b</sup>, R. Jothi Ramalingam<sup>c\*</sup>, H. Lohedan<sup>c</sup>,  
S. Arokiyaraj<sup>d</sup>, S. Yuvaraj<sup>e</sup>, G. Anitha<sup>f</sup>, A. Subramani<sup>g</sup>, K.R. Sunaja Devi<sup>h</sup>,  
M. Sundararajani

<sup>a</sup>Department of Electronics and Communication Engineering, Centurion University of Technology and Management, Odisha, Bhubaneswar-752 050, India

<sup>b</sup>Department of Basic Sciences, College of Fisheries Engineering, Dr. J. Jayalalithaa Fisheries University, Nagapattinam-611 002, India

<sup>c</sup>Department of Chemistry, College of Science, Kind Saud university, Riyadh 11451, Saudi Arabia

<sup>d</sup>Department of Food Science and Biotechnology, Sejong University, South Korea

<sup>e</sup>Department of Physics, Loyola College of Arts and Science, Mettala, Namakkal 636 202, India

<sup>f</sup>Department of Electronics and Communication Engineering, Saveetha University, Chennai, 602 105, India

<sup>g</sup>Department of Chemistry, Apollo Arts and Science College, Poonamallee- 602 105, India.

<sup>h</sup>Department of Chemistry, CHRIST(Deemed to be University), Bangalore, Karnataka-560 029, India

<sup>i</sup>PG & Research Department of Physics, Paavendhar College of Arts & Science, Salem 636 121, India

Employing Microwave combustion technique and utilizing L-arginine as fuel pure Cobalt Aluminate and Zn doped Cobalt Aluminate nanoparticles (NPs) were prepared. XRD, DRS-UV, HRSEM and VSM techniques were used to investigate the structural, optical, morphological, and magnetic properties. The average crystallite size is found in the range of 15 - 24 nm. Elemental confirmation is done by aid of EDX spectra. The band gap values of the produced samples were discovered to be between 2.57 and 2.45 eV. At room temperature, the prepared samples showed diamagnetic magnetic characteristics, which were corroborated by Magnetization–Field (MH) hysteresis curves.

(Received June 23, 2021; Accepted October 15, 2021)

*Keywords:* Cobalt Aluminate, XRD, HR-SEM, DRS-UV and Magnetic analysis

### 1. Introduction

In recent years, researchers have concentrated their efforts on semiconductor nanomaterials due to their unique structural, optical, thermal, electrical, morphological, and magnetic capabilities. Transition metal oxides have excelled in a range of applications, including optical sensors, energy storage, photovoltaic, resistive memory device, capacitor, Resistive RAM and piezoelectricity. [1-4]. Zn doped  $\text{CoAl}_2\text{O}_4$  nanoparticles have been found to exhibit attractive features viz. thermal resistance, improved diffusion, hydrophobicity, low surface acidity, and excellent mechanical resilience. These features make them ideal ideal for sensing applications [5, 6]. Due to the charge carrier and electron mobility, it is also particularly helpful for magnetic and electrical applications [7, 8]. The general formula of zinc doped cobalt aluminate nanoparticles is  $\text{AB}_2\text{O}_4$  (normal spinel structure), where A denotes divalent metal ions ( $\text{Zn}^{2+}$  and  $\text{Co}^{2+}$ ) and B denotes trivalent metal ions ( $\text{Al}^{3+}$ ), implying that divalent ions occupied tetrahedral sites and trivalent metal ions occupied octahedral sites. Cobalt aluminate nanoparticles have been created for a variety of applications, including sol gel, hydrothermal, co-precipitation, combustion, chemical vapour deposition, and polymer precursors [9-16]. For example, the microwave combustion process has several advantages, including a faster synthesis time, reduced costs, and a

---

\* Corresponding author: jrajabathar@ksu.edu.sa

higher yield of zinc doped cobalt aluminate. The fuel/oxidizers principle is employed in propellant chemistry, and nitrates are used as precursors and L-alanine as a fuel. Metal nitrates and fuels employed in this process include citric acid [17], hydrazine [18], glycine, urea [19] and L-arginine [20-23]. During combustion, organic fuels alter the structural, optical, textural, and magnetic properties of the air. The focus of this research is on pure cobalt aluminate and zinc doped cobalt aluminate nanoparticles generated by microwave combustion, with L-arginine as a fuel.

## 2. Experimental Details

### 2.1. Synthesis

$\text{Co}_{1-x}\text{Zn}_x\text{Al}_2\text{O}_4$  ( $x = 0, 0.1, 0.3$  and  $0.5$ ) nanoparticles were synthesised using zinc nitrate ( $\text{Zn}(\text{NO}_3)_2 \cdot 6\text{H}_2\text{O}$ ), cobalt nitrate ( $\text{Co}(\text{NO}_3)_2 \cdot 6\text{H}_2\text{O}$ ), aluminium nitrate ( $\text{Al}(\text{NO}_3)_3 \cdot 9\text{H}_2\text{O}$ ), and L-arginine ( $\text{C}_6\text{H}_{14}\text{N}_4\text{O}_2$ ) (as fuel). All of these high-purity AR-grade compounds were acquired from SD Fine in India and used without further purification [21]. The samples were made with deionized water that had been deionized twice. To make the homogenous solutions, the basic components such as cobalt nitrate/zinc nitrate and aluminium nitrate were mixed together in 1:2 stoichiometric ratios.

The mixed solution was added to the L-arginine solution, which was rapidly agitated for 1 hour.

Metal nitrates were used as oxidizers, and L-arginine was used as fuel. The oxidizer to fuel (O/F) ratio was kept at one according to propellant chemistry law. The combined solutions were then poured into a pair of silica crucibles. To conduct the irradiation process, both silica crucibles were kept separately in two different domestic microwave ovens purchased from SAMSUNG, India Limited. Both microwave ovens were set for 10 minutes at a frequency of 2.54 GHz and an output energy of 900 Watts. Due to the influence of microwave energy, the solution decomposes through processes such as boiling, vaporisation, and dehydration, resulting in the evolution of reaction gas. Ignition took place during the spontaneous combustion phase, resulting in a rapid flame fluffy of  $\text{Co}_{1-x}\text{Zn}_x\text{Al}_2\text{O}_4$  ( $x = 0, 0.1, 0.3$  and  $0.5$ ) nanoparticles NPs. The resulting powder was cleaned with ethanol and deionized water before being calcined for 120 minutes at  $550^\circ\text{C}$ . The powders were created by adding various molar ratios of zinc ( $\text{Zn}^{2+}$ ) to a  $\text{Co}_{1-x}\text{Zn}_x\text{Al}_2\text{O}_4$  nanoparticles spinel structure with  $x = 0, 0.1, 0.3$ , and  $0.5$ , and the samples were labelled (A), (B), (C), and (D), accordingly.

## 3. Results and Discussion

### 3.1. XRD Analysis

The powder XRD diffractograms of the produced  $\text{Co}_{1-x}\text{Zn}_x\text{Al}_2\text{O}_4$  ( $x = 0, 0.1, 0.3$  and  $0.5$ ) nanoparticles nano-aluminates are shown in Fig. 1. The synthesized materials are crystalline, as depicted by the diffractograms.

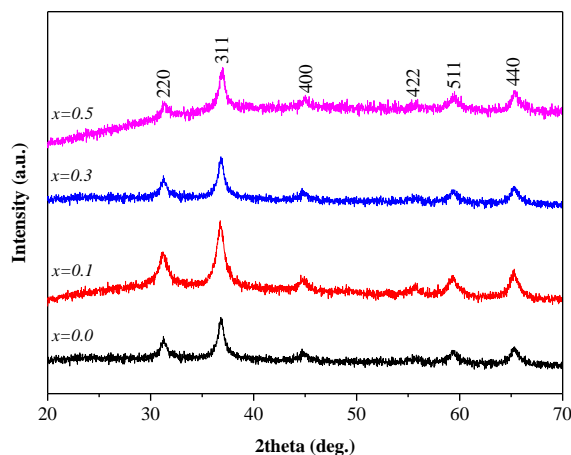


Fig. 1. X-ray diffraction patterns of  $\text{Co}_{1-x}\text{Zn}_x\text{Al}_2\text{O}_4$  ( $x = 0, 0.1, 0.3$  and  $0.5$ ) nanoparticles.

It shows that the prepared NPs have diffracted peaks at 31.17, 36.80, 44.72, 55.50, 59.33, and 65.28, which are perfectly mapped with the (220), (311), (400), (422), (511), and (440) diffraction planes, respectively, and this is further confirmed by matching the diffraction planes with JCPDS card no 82-2239. The presence of cubic spinel structure with space group Fd-3m is confirmed by diffracted Bragg peaks [20]. The purity of the  $\text{CoAl}_2\text{O}_4$  nano-aluminates is ensured by the absence of additional peaks. Using the (311) hkl plane, the average crystallite size ( $L$ ) of the produced  $\text{CoAl}_2\text{O}_4$  and Zn doped  $\text{CoAl}_2\text{O}_4$  nano-aluminates was estimated using Debye Scherrer's Eq. (1).

$$L = \frac{0.89\lambda}{\beta \cos \theta} \quad (1)$$

where,  $L$ - is the average crystallite size,  $\lambda$ -is the wavelength of X-ray source (0.15406 nm),  $\beta$ - is the full width at half maximum (FWHM) of the diffracted peak,  $\theta$ - is the angle of diffraction. For  $x=0$ ,  $x=0.1$ ,  $x=0.3$ , and  $x = 0.5$ , the average crystallite size was found to be 15 nm, 18 nm, 21 nm, and 24 nm, respectively. Using Eq. 2, the lattice parameters of undoped and  $\text{Zn}^{2+}$  doped  $\text{CoAl}_2\text{O}_4$  nanoparticles were calculated.

$$a = d_{hkl} \sqrt{(h^2 + k^2 + l^2)} \quad (2)$$

where,  $d_{hkl}$ - the inter-atomic spacing of the miller indices,  $hkl$ -is the crystal planes,  $a$  - is the lattice parameter.

The calculated lattice parameter 'a' values are quite close to the previously reported values of 8.116, 8.120, 8.126, and 8.135 for  $x=0$ ,  $x=0.1$ ,  $x=0.3$ , and  $x = 0.5$ , respectively [23]. Because the ionic radius of  $\text{Zn}^{2+}$  (0.74) is greater than that of  $\text{Co}^{2+}$  (0.72), the lattice parameter rose linearly with increasing  $\text{Zn}^{2+}$  content [24, 25].

The Williamson-Hall (W-H) plot method was used to measure the effective crystallite size ( $D$ ) and lattice strain ( $\epsilon$ ). W-H equation (3) yields the effective particle size ( $D$ ) and lattice strain ( $\epsilon$ ):

$$\frac{\beta \cos \theta}{\lambda} = \frac{k}{D} + \frac{4\varepsilon \sin \theta}{\lambda} \quad (3)$$

Where  $\lambda$  is the wavelength of the source used,  $\beta$  is full-width half maximum of the diffracted peak,  $\theta$  is the diffracted angle,  $D$  is the crystallite size,  $k$  is the constant and  $\varepsilon$  is the permittivity of free space. The plot is drawn between  $4\sin\theta/\lambda$  vs  $\beta\cos\theta/\lambda$  as shown in Fig.2. The effective crystallite size ( $D$ ) is calculated using the intercept of ( $k/D$ ) on the y-axis, and the lattice strain ( $\varepsilon$ ) is calculated using the slope of the plot. The effective crystallite size value For  $x=0$ ,  $x=0.1$ ,  $x=0.3$ , and  $x = 0.5$ , was found to be 16 nm, 19 nm, 22 nm, and 25 nm, respectively. The lattice strain ( $\varepsilon$ ) value for  $x=0$ ,  $x=0.1$ ,  $x=0.3$ , and  $x = 0.5$ , were deduced 0.079, 0.085, 0.090 and 0.094 respectively. The internal strain induced effective crystallite size causes a deviation in the crystallite size obtained using the Debye-Scherrer formula. The presence of tensile strain in the prepared samples is indicated by the presence of a positive slope (See Fig. 2) [25].

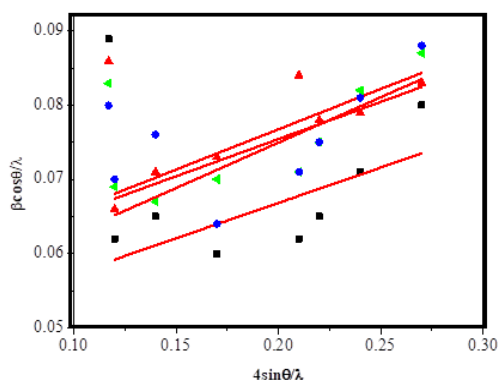


Fig. 2. W-H plot of  $\text{Co}_{1-x}\text{Zn}_x\text{Al}_2\text{O}_4$  ( $x = 0, 0.1, 0.3$  and  $0.5$ ) nanoparticles.

### 3.2 Morphology and Elemental Analysis

HR-SEM was used to examine the form and surface morphology of  $\text{CoAl}_2\text{O}_4$  and Zn doped  $\text{CoAl}_2\text{O}_4$  nanoparticles. We observed coalescence, agglomeration, and large pore diameters in HR-SEM images of  $\text{CoAl}_2\text{O}_4$  and Zn doped  $\text{CoAl}_2\text{O}_4$  nanoparticles, as shown in Figures 3(a)–(d). The presence of high volumes of gases during the combustion process caused the pore size seen in the Zn doped  $\text{CoAl}_2\text{O}_4$  nanoparticle. The existence of elements was confirmed by an energy dispersive X-ray study on  $\text{CoAl}_2\text{O}_4$  and Zn doped  $\text{CoAl}_2\text{O}_4$ . The presence of components such as Co, Al, and O in Figure 4(a) indicates the synthesis of  $\text{CoAl}_2\text{O}_4$  and Zn doped  $\text{CoAl}_2\text{O}_4$  nanoparticles. The presence of elements such as Zn, Co, Al, and O may be seen in Figures 4(b)–(d).

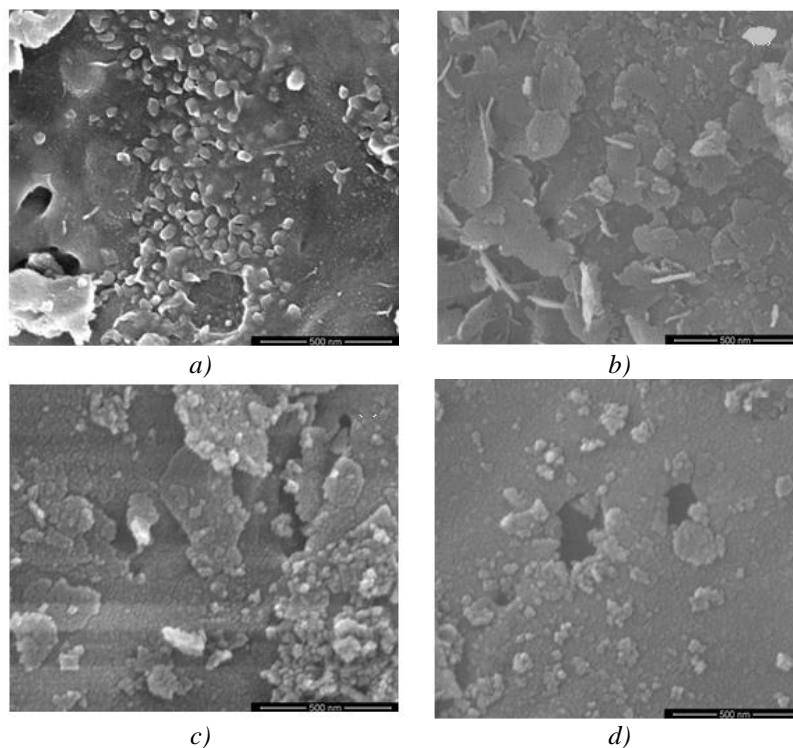


Fig. 3. (a-d) HR-SEM spectra of  $Co_{1-x}Zn_xAl_2O_4$  ( $a=x(0)$ ), ( $b=x(0.1)$ ), ( $c=x(0.3)$ ) and ( $d=x(0.5)$ ) nanoparticles.

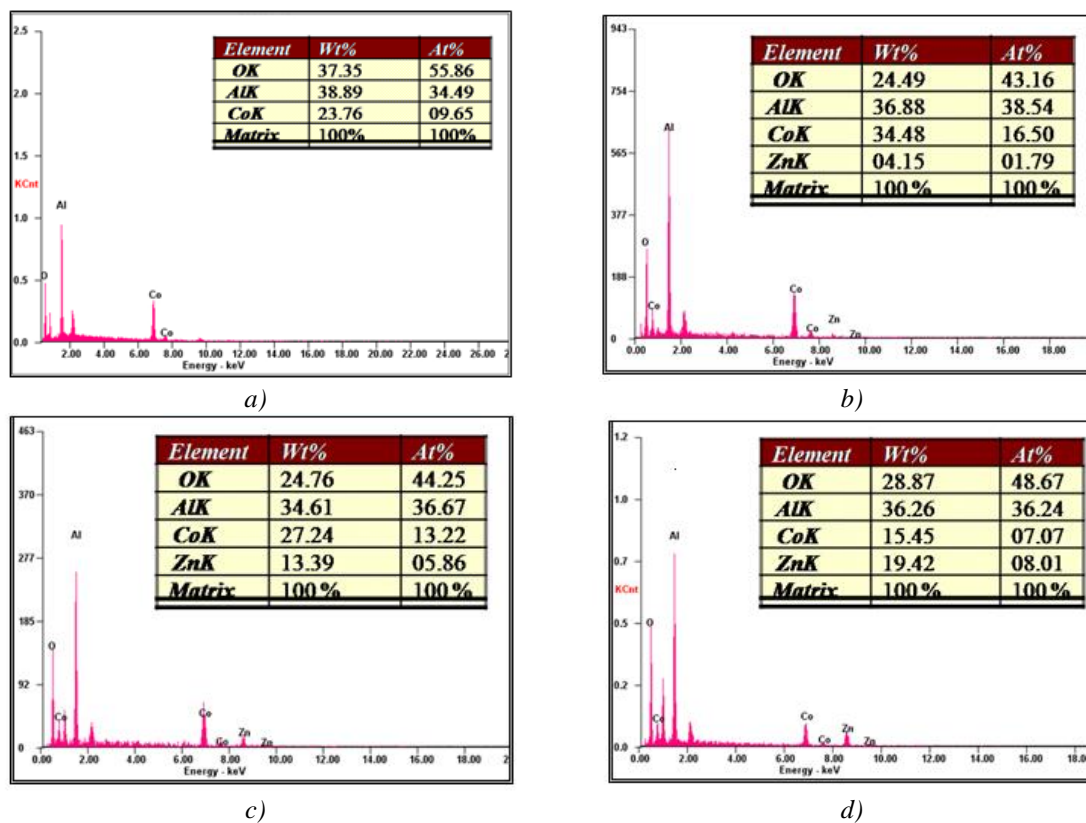


Fig. 4. (a-d) EDAX spectra of  $Co_{1-x}Zn_xAl_2O_4$  ( $x=0$  (a),  $0.1$  (b),  $0.3$  (c) and  $0.5$  (d)) nanoparticles

### 3.3. Bandgap Studies

The optical behaviour of  $\text{CoAl}_2\text{O}_4$  and Zn doped  $\text{CoAl}_2\text{O}_4$  nanoparticles is studied using the UV-DRS instrument. To convert reflectance data into absorption coefficients, the Kubelka-Munk function  $F(R)$  is used.  $F(R)$  is derived using equation (4)

$$\alpha = F(R) = \frac{(1 - R)^2}{2R} \quad \alpha = F(R) = \frac{(1-R)^2}{2R} \quad (4)$$

where,  $\alpha$  - is the absorption coefficient,  $R$  - is reflectance data and  $F(R)$  - is Kubelka-Munk function. As a result, the Tauc relation (equation) is used to calculate the optical band gap (Equ. (5)),

$$F(R)hv = A(hv - E_g)^n \quad (5)$$

where  $n = 2$  denotes the allowable direct transitions and gives the direct band gap, whereas  $n = 1/2$  denotes the permissible indirect transitions and gives the indirect band gap. For the zinc doped cobalt aluminate system, a Tauc plot is shown between  $(F(R)hv)^2$  vs  $hv$  (Fig. 5). The optical bandgap value was calculated using extrapolation of linear points in the Tauc plot  $(F(R)hv)^2$  [21]. The band gap of pure Cobalt aluminate has lately been stated to be 2.57 eV. The direct band gap values for  $\text{Zn}^{2+}$  doped  $\text{CoAl}_2\text{O}_4$  nanoparticles ( $x = 0.0, 0.1, 0.3$ , and  $0.5$ ) were determined to be 2.57, 2.49, 2.47, and 2.45 eV, respectively. Quantum confinement, sp-d exchange interaction between localised d-electrons of Zn divalent ions and band electrons of zinc aluminate in nanoregime resulted in a reduction in band gap energy.

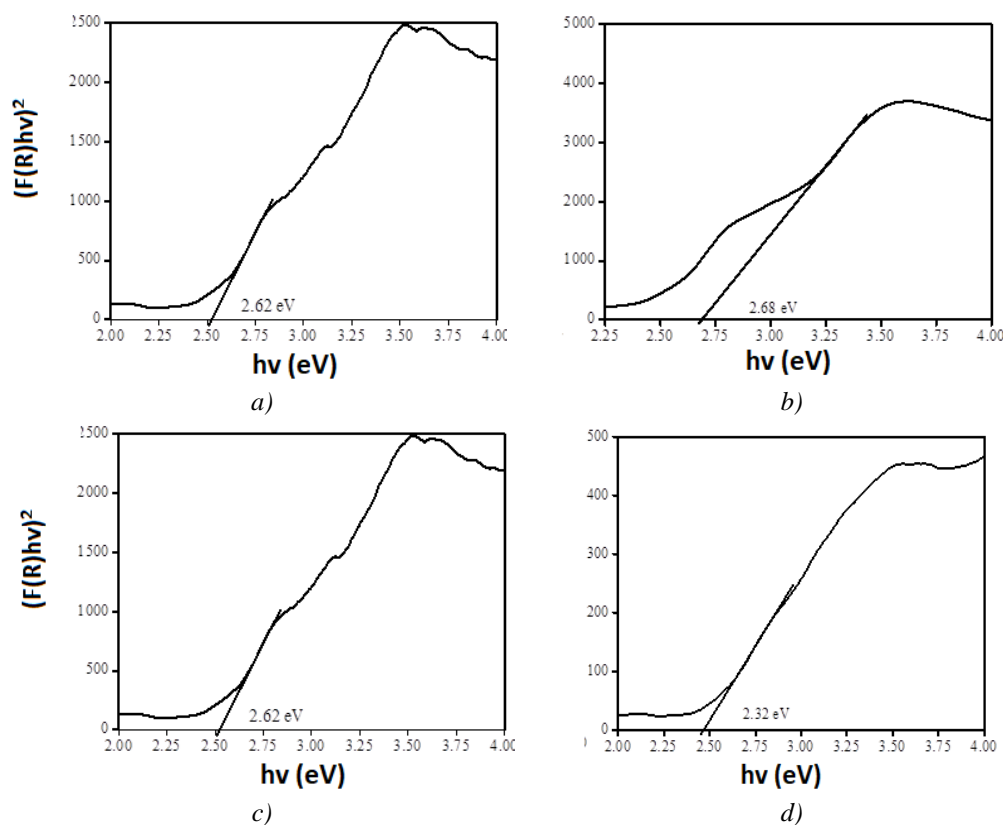


Fig. 5. (a-d)  $(F(R)hv)^2$  versus  $hv$  of  $\text{Co}_{1-x}\text{Zn}_x\text{Al}_2\text{O}_4$  ( $x = 0, 0.1, 0.3$  and  $0.5$ ) nanoparticles

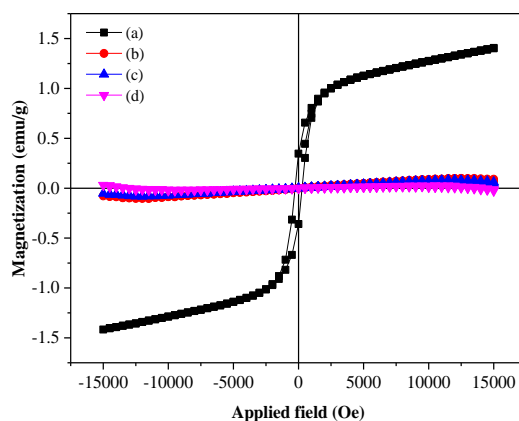
Table 1. Magnetic parameters of  $\text{Co}_{1-x}\text{Zn}_x\text{Al}_2\text{O}_4$  ( $0 \leq x \leq 0.5$ ) nanoparticles.

Sample Name	Sample code	$H_c$ , (Oe)	$M_r$ , (emu/g)
$\text{CoAl}_2\text{O}_4$	(A)	260.17	0.4021
$\text{Co}_{0.9}\text{Zn}_{0.1}\text{Al}_2\text{O}_4$	(B)	110.12	0.0028
$\text{Co}_{0.7}\text{Zn}_{0.3}\text{Al}_2\text{O}_4$	(C)	30.071	0.0033
$\text{Co}_{0.5}\text{Zn}_{0.5}\text{Al}_2\text{O}_4$	(D)	140.65	0.0030

### 3.4. Magnetization analysis

The magnetic characteristics of  $\text{Co}_{1-x}\text{Zn}_x\text{Al}_2\text{O}_4$  ( $x = 0, 0.1, 0.3$  and  $0.5$ ) nanoparticles are determined using VSM experiments. At room temperature, the VSM spectra were obtained between  $-15$  kOe and  $+15$  kOe. Spectra generated between magnetization ( $M$ ) and applied field are shown in Fig. 6. (H). The hysteresis loop was used to collect magnetic properties such as  $H_c$  and  $M_r$ . The cubic spinel structure of  $\text{Co}_{1-x}\text{Zn}_x\text{Al}_2\text{O}_4$  ( $x = 0, 0.1, 0.3$  and  $0.5$ ) nanoparticles was observed, with divalent ( $\text{Co}^{2+}/\text{Zn}^{2+}$ ) metal ions occupying the tetrahedral and trivalent ( $\text{Al}^{3+}$ ) metal ions occupying the octahedral sites, respectively. The cationic redistribution between the tetrahedral and octahedral sites plays an important role in tuning the magnetic characteristics in general.

In this case,  $\text{Co}_{1-x}\text{Zn}_x\text{Al}_2\text{O}_4$  ( $x = 0, 0.1, 0.3$  and  $0.5$ ) nanoparticles exhibit diamagnetic behavior. As seen in Table. 1, it is noted that the value of coercivity ( $H_c$ ) of zinc doped cobalt aluminate nanoparticles lowered upon with rise in the concentration of  $\text{Zn}^{2+}$  ions. It is in the range from 260.17 to 30.07 Oe. The coercivity values can be tuned through various factors like surface defect, cationic redistribution, and high anisotropy [20]. The values of magnetic remanence ( $M_r$ ) are established to be 0.4021 emu/g to 0.0028 emu/g. It is mainly impacted by crystallite size and shape of the  $\text{Zn}^{2+}$  doped  $\text{CoAl}_2\text{O}_4$  nanoparticles.

Fig. 6. (a-d) Magnetic hysteresis curves of  $\text{Co}_{1-x}\text{Zn}_x\text{Al}_2\text{O}_4$  ( $x = 0, 0.1, 0.3$  and  $0.5$ ) nanoparticles.

## 4. Conclusions

Employing Microwave combustion process we successfully synthesised  $\text{Co}_{1-x}\text{Zn}_x\text{Al}_2\text{O}_4$  ( $x = 0, 0.1, 0.3$  and  $0.5$ ) nanoparticles, and all made samples unveiled a cubic spinel structure with space group  $\text{Fd-3m}$ . Furthermore, the Debye-Scherrer and W-H methods were employed to determine the effective crystallite size, with slightly different results. The higher ionic radius of Zn in comparison to Co causes an increase in the values of the lattice parameter from 8.116 to 8.135. With an increase in  $\text{Zn}^{2+}$  concentration, the optical band gap values decrease from 2.57 to 2.45 eV. Vibrational stretching modes in the FT-IR spectra have been connected to the cubic spinel structure of  $\text{CoAl}_2\text{O}_4$ . The produced samples displayed diamagnetic magnetic behaviour, with Remanence ( $M_r$ ) values ranging from 0.4021 emu/g to 0.0028 emu/g, according to magnetization studies.

## Acknowledgments

The authors express thankful and financial support by the Researchers Supporting Project Number (RSP-2021/54) King Saud University, Riyadh, Saudi Arabia.

## References

- [1] B. Behera, S. Maity, A.K. Katiyar, S. Das, Superlattices and Microstructures, 117, 298 (2018).
- [2] D.S.A. Selvan, M. Keerthi, M. Sundararajan, S. Shobana, B. Lakshmi, V. Veena, A.K. Rahiman, Materials Chemistry and Physics, 272, 124903 (2021),
- [3] P. Sakthivel, R.J. Ramalingam, D. Pradeepa, S Rathika, C.S. Dash, K. Bhuvanewari, M. Sundararajan, P.S Subudhi, H.A. Lohedan, Journal of Nanoscience Nanotechnology, 21, 5659, (2021).
- [4] V.R.M. Reddy A. Tony Dhiwahar, S. Maruthamuthu, R. Marnadu, M. Sundararajan, M. Aslam Manthrammele Mohd., Shkir, P. Sakthivel, Solid State Sciences, 113, 106542, (2021).
- [5] T.S. Nirmala, N. Iyandurai, S. Yuvaraj and M. Sundararajan, Materials Research Express, 7, 046104, (2020).
- [6] S. Zhao, J. Guo, W. Li, H. Guo, B. You, Dyes and Pigments, 151, 130 (2018).
- [7] N. Ouahdi, S. Guillemet, J.J. Demai, B. Durand, L.E. Rakho, R. Moussa, A. Samdi, Materials Letters, 59, 334 (2005).
- [8] S. Ramachandran, C.S. Dash, A. Thamilselvan, S. Kalpana, M. Sundararajan, Journal of Nanoscience and Nanotechnology, 20, 2382 (2020).
- [9] S. Salem, S.H. Jazayeri, F. Bondioli, A. Allahverdi, M. Shirvani, A.M. Ferrari, Journal of Applied Ceramic Technology, 9, 968 (2012).
- [10] S. Yuvaraj, A.C. Fernandez, M. Sundararajan, C.S. Dash, P. Sakthivel, Ceramics International, 46, 391 (2020).
- [11] W.S. Cho, M. Kakihana, M. Journal of Alloys and Compounds, 287, 87 (1999).
- [12] M. Sales, C. Valentín, J. Alarcón, Journal of the European Ceramic Society, 17, 41 (1997).
- [13] X. Zhang, F. Shi, X. Yu, H. Liu, Y. Fu, Z. Wang, L. Jiang, X. Li, Journal of the American Chemical Society, 126, 3064 (2004).
- [14] A.G. Soleimani, E. Bakhshandeh, F. Najafi, Journal of the European Ceramic Society, 34, 2959 (2014).
- [15] L. Gama, M.A. Ribeiro, B.S. Barros, R.H.A. Kiminami, I.T. Weber, A.C.F.M Costa, Journal of Alloys and Compounds, 483, 453 (2009).
- [16] M.A.F. Ramalho, L. Gama, S.G. Antonio, C.O.S. Paiva-Santos, E.J. Miola, R.H.G.A. Kiminami, A.C.F.M. Costa, Journal of materials science, 42, 3603 (2007).
- [17] Y.K. Sun, I.H. Oh, S.A. Hong, Journal of materials science, 31, 3617 (1996).
- [18] A. Alarifi, N.M. Deraz, S. Shaban, Journal of Alloys and Compounds, 486, 501 (2009).
- [19] A.T. Raghavender, K. Zadro, D. Pajic, Z. Skoko, N. Biliškov, Materials letters, 64, 1144 (2010).
- [20] A.T. Dhiwahar, M Sundararajan, P Sakthivel, Chandra Sekhar Dash, S Yuvaraj, Journal of Physics and Chemistry of Solids, 138, 109257 (2020).
- [21] A. Roniboss, A. Subramani, R. Ramamoorthy, S. Yuvaraj, M. Sundararajan, C.S. Dash, Materials Science in Semiconductor Processing, 123, 105507 (2021).
- [22] S. Yuvaraj, S. Ramachandran, A. Subramani, A. Thamilselvan, S. Venkatesan, M. Sundararajan, C.S. Dash, Journal of Superconductivity and Novel Magnetism, 33, 1199 (2020).
- [23] C.S. Dash, S.R.S. Prabakaran, Reviews on Advanced Materials Science, 58, 248 (2019).
- [24] D. Gingasu, I. Mindru, L. Patron, L.G. Marinescu, A. Ianculescu, V.A. Surdu, S. Somacescu, S. Preda, O. Oprea, Revue Roumaine Dechimie, 63, 459 (2018).
- [25] H.B. Duvuru, S.K. Alla, S.K. Shaw, S.S. Meena, N. Gupta, B.V. Prasad, M.W. Kothawale, M.K. Kumar, N.K. Prasad, Ceramics International, 45, 16512, (2019).